Optics and Laser Technology 127 (2020) 106185

Contents lists available at ScienceDirect

Optics and Laser Technology

journal homepage: www.elsevier.com/locate/optlastec

604-nm high-order vortex beams directly generated from a Pr:YLF laser with a cavity-loss-induced gain switching mechanism

Saiyu Luo[a], Zhiping Cai[b], Chuanxiang Sheng[a], Li Li[a,*], Qian Chen[a]

[a] School of Electronic and Optical Engineering, Nanjing University of Science and Technology, Nanjing 210094, China
[b] College of Electronic Science and Technology, Xiamen University, Xiamen 361005, China

HIGHLIGHTS

- First demonstration of 604-nm vortices directly generated from a Pr:YLF laser.
- Topological charge up to three was achieved through designated cavity design.
- Cavity-loss-induced gain switching mechanism between 604 and 607 nm emission.
- Output power reached 470, 230, and 60 mW for the 1st-, 2nd-, and 3rd-order vortex.
- Slop efficiencies were 24.5%, 17.5%, and 11.4%, respectively.

ARTICLE INFO

Keywords:
Interference
Laser modes
Optical pumping
Optical resonators

ABSTRACT

In this work, we demonstrated, for the first time to the best of our knowledge, high-order vortex beams at 604 nm that were directly emitted from a Pr:YLF crystal laser. By combining a blue-diode-pumped v-type cavity for controllable Gouy phase introduction and off-axis crystal rotation for high-order HG modes generation, topological charged 604-nm vortex lasers were attained up to the third order. Furthermore, the vortex beams were found to be lasing at 604 nm that was often deemed less prone to lase compared with 607-nm in the same energy manifold. By a detailed spectroscopic study and rate equation analysis, we proposed and confirmed that the 604-nm transition of Pr:YLF crystal could be favorable in the vortex beam generation by a cavity-loss-induced gain switching process, in which the net gain at 604-nm could surpass that of 607-nm as the cavity loss was amassed beyond a threshold value.

1. Introduction

High-order optical vortices, carrying more than one topological charge for each photon, are ideal light sources for macroscopic quantum entanglement measurement [1], angular remote sensing [2], precise spatial measurement [3], and laser printing of chiral plasmonic nanojets [4]. Optical vortices directly generated from lasers, which constitute cavity eigenstates and possess inherently superior beam quality, are preferable choices [5]. Higher-order vortex beams in the orange that is at the absorption band of certain metal phthalocyanines, uranium-doped CaF_2 crystals, and hybrid liposome/Au nanoparticles, may offer new perspectives for applications in nonlinear absorption spectroscopy [6], crystallographic characterization [7], and biomedical photonics [8].

One of the promising and well-studied gain media for orange lasers is the praseodymium-doped yttrium lithium fluoride (Pr:YLF) [9–14]. To realize optical vortex beams, off-axis pumping scheme has been widely used in generating high-order Hermite-Gauss (HG) modes that can be transformed to corresponding high-order Laguerre-Gauss (LG) modes by external mode convertors [15–17]. Such approach was recently exploited to produce red and orange vortex beams directly from a Pr:YLF laser cavity, however, the vortices achieved were limited to first-order vortex beams [18,19].

In this paper, we demonstrated direct emission of high-order LG vortex beams in the orange spectra from a Pr:YLF laser utilizing an equivalent off-axis pumping scheme combined with a robust $\pi/2$ Gouy phase introduction. Furthermore, upon studying the emitted spectra of LG vortex beams up to the 3rd order, we discovered that the wavelength was centered at 604 nm, instead of the commonplace 607 nm in the orange. Based on a thorough spectroscopic study and rate-equation analysis, we confirmed that, to the contrary of common notions, the net gain of 604-nm transition at room temperature could be higher than

* Corresponding author.
E-mail address: lili@njust.edu.cn (L. Li).

https://doi.org/10.1016/j.optlastec.2020.106185
Received 3 December 2019; Received in revised form 22 February 2020; Accepted 25 February 2020
Available online 29 February 2020
0030-3992/

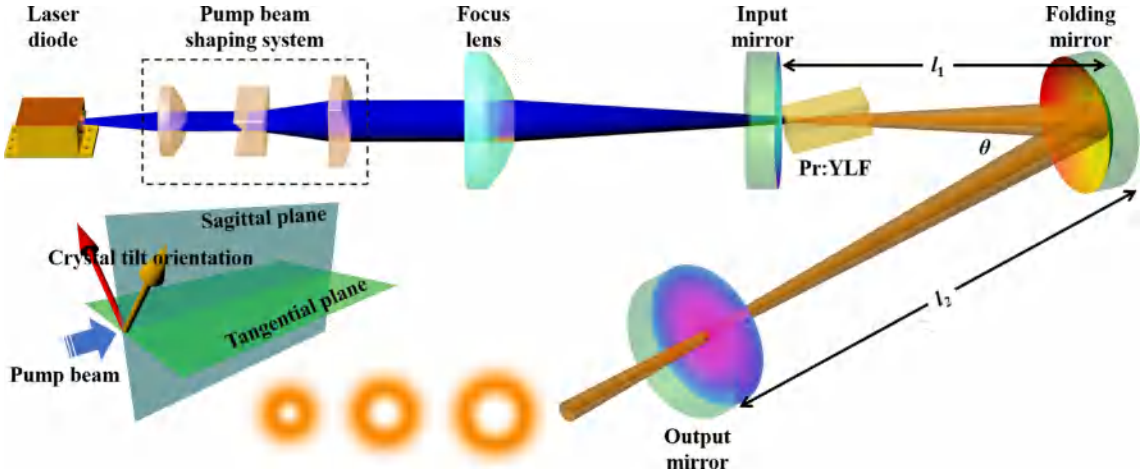

Fig. 1. Schematic setup of the blue-diode-pumped 604-nm vortex laser with topological charge up to 3.

that of 607-nm by a simple cavity loss management when the total loss was beyond a threshold value, resulting in a swift gain switching from 607 to 604 nm with the proper setup.

2. Experimental setup

To directly generate orange LG vortex beams, as illustrated in Fig. 1, we utilized a three-mirror v-type Pr:YLF cavity. The gain medium was a cubic *a*-cut crystal with a relatively low doping concentration of 0.3 at. %. The low doping level was to not only reduce the thermal load and avoid the risk of crystal fracturing [14], but also weaken the ground-state re-absorption [10]. A relatively large crystal thickness of 10 mm was consequently utilized to increase the pump absorption. The Pr:YLF crystal was polished at both ends, wrapped in indium foils on the side, and mounted on a copper heatsink that was Peltier cooled to 12 °C. The crystal was integrated onto a kinematic mount with two motorized actuators, which provided an angular precision of 6 arc second to stimulate the high-order transverse modes. The pump diodes and beam shaping system were similar as in [20], except that the diode temperature was set at 21 °C to optimize pump absorption. The v-type cavity was carefully constructed to effectively introduce an appropriate Gouy phase difference to high-order beams, which was critical for the HG to LG mode conversion [21]. The planar input mirror (IM) was coated with high transmission (> 98%) from 436 to 455 nm for the pump, and transmission of 72% at 522 nm to suppress possible lasing. The IM was also highly reflective (> 99.8%) from 592 to 620 nm. The folding mirror (FM) was coated of high reflection (> 99.8%) from 560 to 611 nm and high transmission (> 60%) from 631 to 738 nm to suppress possible lasing at 640 and 721 nm. The third mirror, partially reflective with ~13.6% transmission from 600 to 610 nm, was chosen as the output mirror (OM). To characterize the output beam, an improved Fizeau interferometer [22] in the orange spectral region was utilized to generate spherical wave interference, which was followed with a neutral density filter and a high-resolution CCD camera for interferogram recording.

3. Results and discussion

For vortex beam generation, LG modes can be converted from HG modes by superimposing a π/2 Gouy phase, while HG modes can be acquired by lowering the threshold below that of Gaussian mode with proper crystal rotation [23]. The set of cavity parameters, l_1, l_2, and θ, required to bring the π/2 Gouy phase into the laser, can be calculated by the ABCD matrix law [21] with results plotted in Fig. 2(a). In general, l_1 increases with the decrease of θ, and l_2 increases with both l_1 and θ decreasing. On the other hand, the value of θ is closely related to

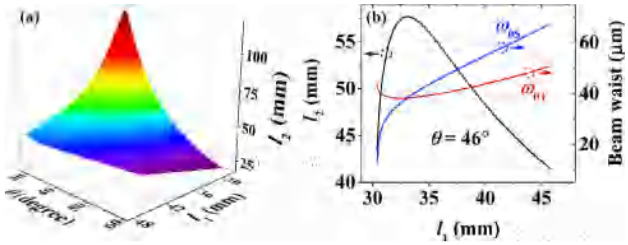

Fig. 2. Cavity parameters design for π/2 Gouy phase shift. (a) Relationship among cavity parameters l_1, l_2, and θ; (b) Variation of l_2 and signal beam waist versus l_1.

the cavity modal size. To achieve higher laser efficiency, the signal beam inside the gain crystal should be optimized for maximal overlapping with the pump beam. Thus in our design, θ was chosen to be 46°. The variation of l_2 and tangential/sagittal waist radius (ω_{0T}/ω_{0S}) in the crystal versus l_1 were plotted in Fig. 2(b). It was revealed that a maxima of $l_2 \approx 58$ mm existed at $l_1 \approx 33$ mm, resulting in $\omega_{0T} = \omega_{0S} \approx 38$ μm that matched well with the pump mode inside. Therefore, l_1 and l_2 were set at around 33 and 58 mm, respectively, to initiate the vortex beam lasers.

A. First-order vortex beam generation

To initiate the laser operation, TEM_{00} mode (Fig. 3(a)) was first obtained by aligning the end surfaces of Pr:YLF crystal perpendicular to the pump beam and adjusting IM and OM near the FM center. Next, by consecutively rotating the crystal both in the tangential and sagittal plane by an angle of ~2.2°, i.e., indicated by the orange arrow in the bottom left inset in Fig. 1, the diagonal HG_{01} mode (Fig. 3(c)) was achieved. In the next step, l_1 and l_2 were set at the calculated values and

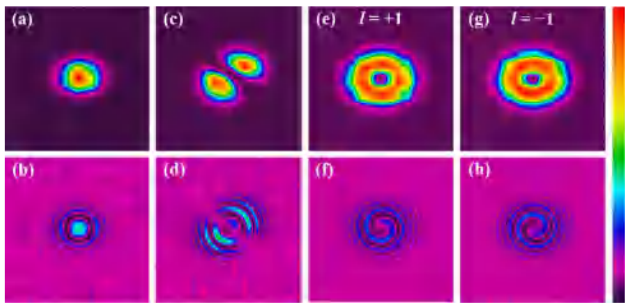

Fig. 3. The intensity profiles and corresponding interferograms for (a, b): TEM_{00}; (c, d): diagonal HG_{01}; (e, f): $LG_{0,+1}$; and (g, h): $LG_{0,-1}$ modes.

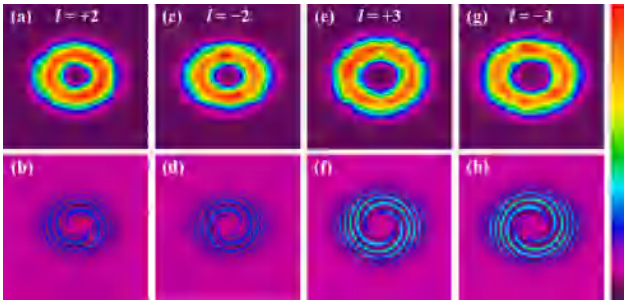

Fig. 4. The intensity profiles and corresponding interferograms for (a, b): $LG_{0,+2}$; (c, d): $LG_{0,-2}$; (e, f): $LG_{0,+3}$; and (g, h) $LG_{0,-3}$ modes.

gradually adjusted. The output pattern was monitored in situ for the LG_{01} mode appearance. The doughnut-shaped pattern (Fig. 3(e)) was achieved, as expected, when l_1 and l_2 were adjusted to ~34 and 56 mm, respectively. The corresponding interferogram of distinctly clockwise helical fringes was observed (Fig. 3(f)), which revealed a spiral phase wavefront and confirmed a vortex beam with topological charge $l = +1$. Later, the crystal was rotated in the opposite tangential plane by the same angle and an annular pattern (Fig. 3(g)) with anticlockwise helical interferogram (Fig. 3(h)) was obtained. It presented an inverse handedness ($l = -1$) and confirmed the validity of controllable chirality with our vortex lasers. The interferograms of TEM_{00} and diagonal HG_{01} modes were also inspected and displayed in Fig. 3(b) and (d), respectively, both of which exhibited ring-shaped interference patterns with no spiral structure and indicated zero carried OAM.

B. High-order vortex beam generation

Moving forward with the 1st-order vortices, we further rotated the YLF crystal and adjusted the cavity parameters to achieve high-order vortex beams. The 2nd-order vortex beam, as shown in Fig. 4(a), was observed when the total tilt angle was tuned to 5.4°, while l_1, l_2, and θ were adjusted to ~33 mm, 59 mm, and 45°, respectively. The 3rd-order vortex beam, as shown in Fig. 4(e), was observed when the total tilt angle was tuned to 6.8°, while l_1, l_2, and θ were adjusted to ~32 mm, 64 mm, and 44°, respectively. The corresponding interference patterns illustrated very clear spiral fringes with both topological charge $l = +2$ in Fig. 4(b), and $l = +3$ in Fig. 4(f). Furthermore, the handedness of vortices were also inverted in a similar manner as the 1st-order modes. The beam spots of $LG_{0,-2}$ and $LG_{0,-3}$ modes were shown in Fig. 4(c) and (g), respectively. Their interference patterns were displayed in Fig. 4(d) and (h), respectively. We noted a small ellipticity existed in the beam spots and we believed it was due to the astigmatism caused by the cavity folding and crystal rotation. We also noted that in achieving a larger topological charge, l_1 and θ were decreased slightly while l_2 was increased larger than l_1. Such experimental observations were consistent with our theoretical predictions in Fig. 2(a).

C. The laser emission spectrum and power

In recording the emission spectra of vortex lasers, an intriguing observation was revealed during mode conversion. First, the central emission wavelength was located at 607.0 nm for the TEM_{00} mode, as expected; however, it was shifted to 604.2 nm for the HG_{01} and LG_{01} (both chiralities) modes as well as higher topological charges up to the 3rd order, as shown in Fig. 5(a). As we mentioned earlier, such an abrupt switch in the emitted spectra was against the common observations for regular orange lasers with Pr:YLF crystals. The physical explanation to this interesting phenomenon will investigated in detail in the next section.

Regarding the emitted vortex laser power, the maximum continuous-wave (cw) output power for the 1st-, 2nd-, and 3rd-order 604-nm laser reached 470, 230, and 60 mW, respectively, under an absorbed pump of 2.8 W. The pump thresholds were 0.76, 1.46, and 2.29 W, respectively, and accordingly the slop efficiencies were 24.5%, 17.5%, and 11.4%, respectively. All three outputs exhibited no obvious thermal rollover and were only limited by the available pump power, as shown in Fig. 5(b). The degradation of laser efficiencies for higher-order vortex modes could be attributed to two main reasons. The first was that higher-order vortex beams had larger hollow areas and smaller mode sizes inside the gain crystal, which reduced the signal-pump overlapping efficiency. The second was due to the higher diffraction losses at the crystal surfaces for higher-order modes with larger tilt angles.

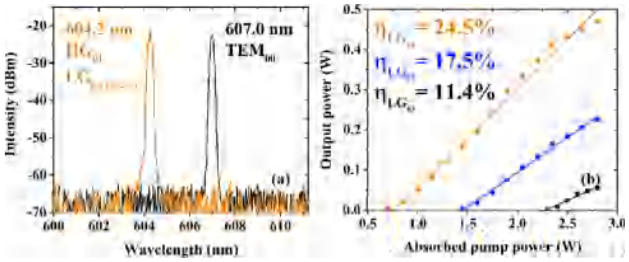

Fig. 5. (a) The emission spectra of the orange lasers in the TEM_{00} (black) and vortex (orange) modes. (b) The output versus absorbed pump for the 604-nm vortex lasers.

4. Validation of the cavity-loss-induced gain switching and emission spectrum change

The switching of the emitted laser spectrum from 607 to 604 nm along with the vortex beam occurrence has led us to investigate on the spectroscopic characteristics in Pr:YLF lasing. It is well known that Pr:YLF crystal has two close emission peaks in the same energy manifold at 604 and 607 nm, respectively [11]. Traditionally, the perception is that the 607-nm transition is prone to lasing because it has higher gain and lower loss comparing with those of 604-nm [12]. This preconceived notion has been supported by several experimental observations [13,14] including the recently demonstrated Pr:YLF vortex laser at 607 nm [18]. On the other hand, for Pr:YLF to laser at 604 nm, extra resources have to be employed including cryogenic facilities [9], Fabry–Perot etalons [10], and saturable absorbers [24] etc., resulting in complex, costly, and less efficient laser systems. There has been little reported studies for a room-temperature Pr:YLF laser preferentially emitting at 604 nm without some delicate external measures.

We first looked into the polarization-resolved spectroscopy for the $^3H_4 \rightarrow {}^1D_2$ ground-state absorption and $^3P_0 \rightarrow {}^3H_6$ emission processes to characterize the transition strength at 604 and 607 nm. The absorption spectra were completed with a visible spectrophotometer (PerkinElmer Inc., Lambda 850). Although this absorption was considered spin forbidden and non-resonant with low cross-sections [12,13], our inspection revealed the absorption cross-sections at 604 and 607 nm were 6.7×10^{-22} cm^2 and 1.2×10^{-22} cm^2, respectively, which were consistent with previous reports [12]. Next, the emission spectra were carefully recorded by pumping a cubic Pr:YLF crystal at one edge and collecting the emission from a perpendicular side to minimize possible re-absorption. The emission data were recorded with an optical spectrum analyzer (Yokogawa, AQ6373B) in the visible and the emission cross-sections were derived to be 19.6×10^{-20} cm^2 and 15.7×10^{-20} cm^2 at 604 and 607 nm, respectively. To note, our emission cross-section at 604 nm was double as previously reported data [13], while similar at 607 nm. Our spectroscopic data indicated that while the 604-nm transition possibly possessed a slightly higher gain, the 607-nm gain was substantially less (~5 times less) influenced by the ground-state absorption. This inherent absorption could be substantial and effectively prevent the 604-nm lasing with 607-nm gain present. This

perspective was obviously met with earlier results [13] where cw 607-nm lasing first occurred at a low pump level, and cw 604-nm lasing appeared only after the pump exceeded a high level such that both transitions could overcome the inherent losses from the ground-state absorption.

To understand the gain competition process between the two orange wavelengths, a generic rate equation analysis was conducted, as listed in Eq. (1), with an assigned general cavity loss γ [25]. The photon density is ϕ, the excited-state population density is N_E, the ground-state population density is N_G, and $N = N_E + N_G$ is the total Pr^{3+} population density. The subscripts 1 and 2 denote the 604- and 607-nm transition, respectively.

$$\begin{cases} \frac{d\phi_1}{dt} = \frac{\phi_1}{t_c}[2L(\sigma_{e1}N_E - \sigma_{a1}N_G) - \gamma], \\ \frac{d\phi_2}{dt} = \frac{\phi_2}{t_c}[2L(\sigma_{e2}N_E - \sigma_{a2}N_G) - \gamma], \\ \frac{dN_E}{dt} = \frac{\sigma_{ap}\lambda_p P_p}{hc\pi\omega_p^2}N_G - (\phi_1\sigma_{e1} + \phi_2\sigma_{e2})cN_E - \frac{N_E}{\tau_f}, \end{cases} \quad (1)$$

In the rate equations, t_c is the cavity round-trip time, L is the crystal length, c is the speed of light in vacuum, and τ_f is fluorescence lifetime. Here σ_e and σ_a denote the emission and absorption cross-section, respectively. For the pump laser, λ_p, P_p, σ_{ap}, and ω_p are the wavelength, absorbed power, absorption cross-section, and beam radius inside the crystal, respectively. Base on the rate-equation set, we simulated the gain competition process between the two transition lines with parameters listed in Table 1.

The simulation results, i.e., the photon density versus loss term γ, were plotted in Fig. 6. It was clearly observed there existed a steep turning point that triggered the gain switching between 604- and 607-nm transitions. The critical loss γ was found at 17.3%, depending on the parameters chosen. Note that it was the only switching point for γ from zero to 100%, as shown in the inset of Fig. 6, and the 604-nm gain prevailed afterwards. This general loss γ was mainly composed of the reflection and absorption losses from the crystal, and output coupler loss. The obtained critical loss provided a good guideline for the subsequent vortex laser design aiming at 604-nm high-order modes with expected higher cavity loss.

To validate the theoretical predication with our experimental observations, we hereby looked into the detailed losses in our cavity set. For the TEM_{00} mode with collinear alignment, the reflected beam at the crystal facet was always injected back into the cavity that led to a maximal internal loss below 1% for a well-aligned cavity [27]. The utilized OM transmittance was 13.6%, thus for the TEM_{00} mode the cavity loss was about 15.6%, which was below the critical loss of 17.3% and in favor of 607-nm transition. On the other hand, high-order transverse modes, including the 1st- and higher-order vortices, generally experienced more severe losses by the tilted crystal and cavity mirrors. In a cavity round-trip, the laser beam would pass through the crystal facets for a total of four times. Since the crystal was tilted, part of the reflected beam would eventually exit the resonator after a few bounces. The total reflection loss, considering the Fresnel reflection was ~3.7% at one Pr:YLF crystal facet (uncoated with a refractive index of 1.476 at 604 nm and 1.453 at 607 nm) and the small tilt angle, was estimated to be no less than 4% under proper assumption. Thus, the total cavity loss was amassed to be 18.6% or higher, which was beyond the threshold in favor of the 604-nm transition. Therefore, our experimental observations were in good agreement with the theoretical predictions. Without this loss management, vortex beams would still emit at the preferable 607 nm in a simple linear cavity [18].

Table 1
Parameters utilized in the rate equations.

Parameter	Value	Unit	Parameter	Value	Unit
L	10	mm	σ_{ap}	9.0×10^{-20} [12]	cm^2
t_c	0.63	ns	λ_p	444	nm
τ_f	38 [26]	fs	P_p	2.8	W
N	4.2×10^{19}	cm^{-3}	ω_p	40.5	μm
σ_{e1}	19.6×10^{-20}	cm^2	σ_{a1}	6.7×10^{-22}	cm^2
σ_{e2}	15.7×10^{-20}	cm^2	σ_{a2}	1.2×10^{-22}	cm^2

Note: the listed parameters are based on the laser design in Fig. 1.

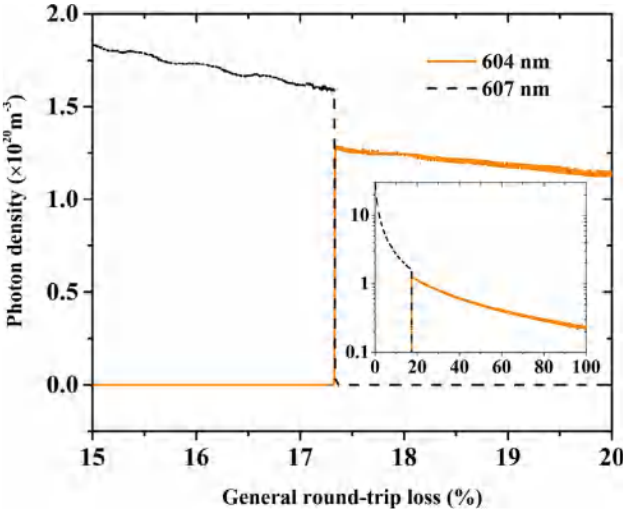

Fig. 6. The gain switching process between the 604- and 607-nm transitions versus round-trip loss γ.

5. Conclusion

To conclude, in this paper we presented a diode-pumped Pr:YLF laser that directly generated high-order vortex laser beams at 604 nm. Utilizing an elaborate design to superpose an intra-cavity π/2 Gouy phase shift and a delicate cavity loss management that preferred the 604-nm transition line, LG vortex laser emissions of both chiralities were achieved from HG modes conversion. Vortex beams up to the 3rd-order were attained directly out of the laser cavity with appreciable maximal output powers of 470, 230, and 60 mW for the 1st-, 2nd-, and 3rd-order, respectively. We validated the emission wavelength at 604 nm of the vortex beams by a thorough spectroscopic study and rate-equation analysis in the orange laser transition, and revealed that by a controlled loss mechanism the 604-nm transition could have a stronger net gain than that of the 607-nm for the direct vortex lasers. Further exploration to achieve even higher-charged vortices extending to visible wavelengths such as green and deep red, as well as to pulsed laser operations are currently ongoing.

CRediT authorship contribution statement

Saiyu Luo: Conceptualization, Methodology, Software, Formal analysis, Investigation, Writing - original draft, Visualization. **Zhiping Cai:** Validation. **Chuanxiang Sheng:** Resources, Funding acquisition. **Li Li:** Writing - review & editing, Supervision, Funding acquisition, Project administration. **Qian Chen:** Resources, Funding acquisition.

Declaration of Competing Interest

The authors declare that they have no known competing financial interests or personal relationships that could have appeared to influence the work reported in this paper.

Acknowledgement

This work is supported by NSAF (No. U1830123), the National Natural Science Foundation of China (No. 61627802), the Natural Science Foundation of Jiangsu Province (No. BK20180460), and the

High-Level Educational Innovation Team Introduction Plan of Jiangsu, China.

References

[1] R. Fickler, G. Campbell, B. Buchler, P.K. Lam, A. Zeilinger, Quantum entanglement of angular momentum states with quantum numbers up to 10,010, Proc. Natl. Acad. Sci. U. S. A. 113 (2016) 13642–13647.

[2] R. Fickler, R. Lapkiewicz, W.N. Plick, M. Krenn, C. Schaeff, S. Ramelow, A. Zeilinger, Quantum entanglement of high angular momenta, Science 338 (2012) 640–643.

[3] O. Emile, J. Emile, Naked eye picometer resolution in a Michelson interferometer using conjugated twisted beams, Opt. Lett. 42 (2017) 354–357.

[4] T. Omatsu, K. Miyamoto, K. Toyoda, R. Morita, Y. Arita, K. Dholakia, A new twist for materials science: the formation of chiral structures using the angular momentum of light, Adv. Opt. Mater. 7 (2019) 1801672.

[5] Z. Qiao, G. Xie, Y. Wu, P. Yuan, J. Ma, L. Qian, Dianyuan Fan, Generating high-charge optical vortices directly from laser up to 288th order, Laser Photon. Rev. 12 (2018) 1800019.

[6] K.P. Unnikrishnan, Jayan Thomas, V.P.N. Nampoori, C.P.G. Vallabhan, Nonlinear absorption in certain metal phthalocyanines at resonant and near resonant wavelengths, Opt. Commun. 217 (2003) 269–274.

[7] L. Su, W. Yang, J. Xu, Y. Dong, G. Zhou, Optical absorption properties and valence states of uranium in CaF_2 crystals grown by TGT, J. Cryst. Growth 270 (2004) 150–155.

[8] J.-H. Lee, Y. Shin, W. Lee, K. Whang, D. Kim, L.P. Lee, et al., General and programmable synthesis of hybrid liposome/metal nanoparticles, Sci. Adv.e1601838 2 (2016).

[9] M. Fibrich, J. Šulc, H. Jelínková, Pr:YLF orange laser investigation at cryogenic temperature, Laser Phys. Lett. 12 (2015) 095801.

[10] Y. Cheng, B. Xu, B. Qu, S. Luo, H. Yang, H. Xu, et al., Comparative study on diode-pumped continuous wave laser at 607 nm using differently doped Pr^{3+}:$LiYF_4$ crystals and wavelength tuning to 604 nm, Appl. Optics 53 (2014) 7898–7902.

[11] Z. Liu, B. Qu, J.L. Doualan, B. Xu, H. Xu, Z. Cai, et al., Temperature effects on the main absorption and emission lines of the Pr^{3+}:$LiYF_4$ laser crystal, J. Opt. Soc. Am. B 32 (2015) 263–269.

[12] B. Xu, Z. Liu, H. Xu, Z. Cai, C. Zeng, S. Huang, et al., Highly efficient InGaN-LD-pumped bulk Pr:YLF orange laser at 607 nm, Opt. Commun. 305 (2013) 96–99.

[13] P.W. Metz, F. Reichert, F. Moglia, S. Müller, D.-T. Marzahl, C. Kränkel, et al., High-power red, orange, and green Pr^{3+}:$LiYF_4$ lasers, Opt. Lett. 39 (2014) 3193–3196.

[14] H. Tanaka, S. Fujita, F. Kannari, High-power visibly emitting Pr^{3+}:YLF laser end pumped by single-emitter or fiber-coupled GaN blue laser diodes, Appl. Optics 57 (2018) 5923–5928.

[15] Y. Shen, Y. Meng, X. Fu, M. Gong, Wavelength-tunable Hermite-Gaussian modes and an orbital-angular-momentum-tunable vortex beam in a dual-off-axis pumped Yb:CALGO laser, Opt. Lett. 43 (2018) 291–294.

[16] P.H. Tuan, Y.H. Hsieh, Y.H. Lai, K.F. Huang, Y.F. Chen, Characterization and generation of high-power multi-axis vortex beams by using off-axis pumped degenerate cavities with external astigmatic mode converter, Opt. Express 26 (2018) 20481–20491.

[17] N. Li, B. Xu, S. Cui, X. Qiu, Z. Luo, H. Xu, et al., High-order vortex generation from CW and passively Q-switched Pr:YLF visible lasers, IEEE Photonic. Tech. L. 31 (2019) 1457–1460.

[18] Y. Ma, A. Vallés, J.-C. Tung, Y.-F. Chen, K. Miyamoto, T. Omatsu, Direct generation of red and orange optical vortex beams from an off-axis diode-pumped Pr^{3+}:YLF laser, Opt. Express 27 (2019) 18190–18200.

[19] N. Li, J. Huang, B. Xu, Y. Cai, J. Lu, L. Zhan, et al., Direct generation of an ultrafast vortex beam in a CVD-graphene-based passively mode-locked Pr:$LiYF_4$ visible laser, Photon. Res. 7 (11) (2019) 1209–1213.

[20] S. Luo, Z. Cai, H. Xu, Z. Shen, H. Chen, L. Li, et al., Direct oscillation at 640-nm in single longitudinal mode with a diode-pumped Pr:YLF solid-state laser, Opt. Laser Technol. 116 (2019) 112–116.

[21] S. Wang, S. Zhang, H. Yang, J. Xie, S. Jiang, G. Feng, et al., Direct emission of chirality controllable femtosecond LG_{01} vortex beam, Appl. Phys. Lett. 112 (2018) 201110.

[22] S. Cui, B. Xu, S. Luo, H. Xu, Z. Cai, Z. Luo, et al., Determining topological charge based on an improved Fizeau interferometer, Opt. Express 27 (2019) 12774–12779.

[23] X. Huang, B. Xu, S. Cui, H. Xu, Z. Cai, L. Chen, Direct generation of vortex laser by rotating induced off-axis pumping, IEEE J. Sel. Top. Quant. 24 (2018) 1601606.

[24] Y. Cheng, J. Peng, B. Xu, H. Xu, Z. Cai, J. Weng, Passive Q-switching of Pr:$LiYF_4$ orange laser at 604 nm using topological insulators Bi_2Se_3 as saturable absorber, Opt. Laser Technol. 88 (2017) 275–1259.

[25] O. Svelto, Principles of Lasers, fifth ed., Springer, 2010.

[26] A. Richter, E. Heumann, E. Osiac, G. Huber, W. Seelert, A. Diening, Diode pumping of a continuous-wave Pr^{3+}-doped $LiYF_4$ laser, Opt. Lett. 29 (2004) 2638–2640.

[27] T. Gün, P. Metz, G. Huber, Power scaling of laser diode pumped Pr^{3+}:$LiYF_4$ CW lasers: efficient laser operation at 522.6 nm, 545.9 nm, 607.2 nm, and 639.5 nm, Opt. Lett. 36 (2011) 1002–1004.